Available online at www.sciencedirect.com
SCIENCE DIRECT
Journal of Nuclear Materials 349 (2006) 304–316
journal of nuclear materials
www.elsevier.com/locate/jnucmat

Behavior of thorium–uranium (IV) phosphate–diphosphate sintered samples during leaching tests. Part II. Saturation processes

N. Clavier [a], E. du Fou de Kerdaniel [a], N. Dacheux [a,*], P. Le Coustumer [b], R. Drot [a], J. Ravaux [c], E. Simoni [a]

[a] *Groupe de Radiochimie, Institut de Physique Nucléaire, Bât.100, Université Paris-Sud-11, 91406 Orsay, France*
[b] *CDGA, Université de Bordeaux I, BP 19, Avenue des facultés, 33405 Talence, France*
[c] *LCSM, Université H. Poincaré – Nancy I, BP 239, 54506 Vandoeuvre lès Nancy, France*

Accepted 18 November 2005

Abstract

Sintered pellets of thorium–uranium (IV) phosphate–diphosphate solid solutions (β-$Th_{4-x}U_x(PO_4)_4P_2O_7$, β-TUPD) were altered in several acidic media. All the results reported in the first part of this paper confirmed the good chemical durability of the samples. The evolution of the normalized weight loss showed that, in several media, thorium quickly precipitates in a neoformed phosphate-based phase while uranium (IV) is released in the leachate due to its oxidation into the uranyl form. The characterization of neoformed phases was carried out through several techniques involving grazing XRD, infrared and μ-Raman spectroscopies, EPMA, SEM and TEM. SEM micrographies showed that the dissolution mainly occurs at the grain boundaries, leading to the break away of the grains: only the first 15 μm are altered for 2 months in 10^{-1} M HNO_3. From EPMA and BET measurements, neither the chemical composition nor the specific surface area are significantly modified. Near equilibrium, two neoformed phases were observed and identified by grazing XRD and/or μ-Raman spectroscopy at the surface of the leached pellets: one is found to be amorphous and progressively turns into the crystallized thorium phosphate–hydrogenphosphate hydrate (TPHPH). From the results obtained, a chemical scheme of the dissolution of β-TUPD sintered samples is proposed. The behavior of the actinides in the gelatinous phase appears mainly driven by their oxidation state: thorium remains in the tetrapositive state and is quickly and quantitatively precipitated while uranium (IV) is oxidized into uranyl then released in the leachate. The Th-precipitation as TPHPH first appears scattered then covers the entire surface of the pellet, inducing a delay of the actinides release in the leachate. Both phases act as protective layers and should induce the significant delay of the release of actinides (Th, U) to the biosphere.

1. Introduction

Several phosphate materials such as apatites ($Ca_{10}(PO_4)_6F_2$) [1,2], monazites ($LnPO_4$) and associated brabantites ($M^{II}M^{IV}(PO_4)_2$) [3–9], or thorium phosphate–diphosphate [10–15] have been

DOI of original article: 10.1016/j.jnucmat.2005.11.009
* Corresponding author. Tel.: +33 1 69 15 73 46; fax: +33 1 69 15 71 50.
E-mail address: dacheux@ipno.in2p3.fr (N. Dacheux).

0022-3115/$ - see front matter © 2005 Elsevier B.V. All rights reserved.
doi:10.1016/j.jnucmat.2005.11.010

extensively studied as potential candidates for the immobilization of radionuclides and especially actinides. All these materials exhibit easy ways of preparation, good sintering capability associated to a strong resistance to irradiation and to aqueous alteration. On the basis of some physico-chemical properties, the thorium phosphate–diphosphate (β-$Th_4(PO_4)_4P_2O_7$, β-TPD) appears as a promising material for the specific immobilization of actinides. This solid was prepared either in the powdered form by wet or dry chemical processes [11,16] or as dense sintered pellets (94–99% of the calculated value) through a rather simple two-step procedure involving an uniaxial pressing at room temperature then a heat treatment at 1250 °C [17,18].

The first part of this study [19], based on a kinetic approach, was performed on β-TUPD sintered samples through leaching tests in several media and showed that the sintering process did not affect significantly the dissolution of the materials. Indeed, all the normalized dissolution rates determined (between 10^{-7} and 10^{-4} g m^{-2} day^{-1}) were consistent with that previously obtained for powdered samples [15,20] and appear several orders of magnitude slower than that of other matrices such as basaltic glasses [21]. Moreover, the dissolution of β-TUPD pellets was rapidly followed by the precipitation of phosphate-based neoformed phases in several media considered.

While the first part of this study was principally dedicated to the kinetics of the β-TUPD dissolution, the results reported in this paper are mainly focused on the thermodynamic approach through the identification and the complete characterization of the phases neoformed in the back-end of the initial dissolution reaction. In this objective, the leached samples were observed and extensively investigated by the means of various physico-chemical techniques such as SEM, TEM, EPMA, grazing XRD and spectroscopic ones like XPS and TRLIFS. On the basis of the results obtained, a chemical scheme of dissolution of β-TUPD sintered samples is proposed.

2. Experimental

2.1. Chemicals and apparatus

All the reagents, except uranium and thorium solutions, were supplied by VWR or Aldrich and were of pro-analysis grade. Uranium metal chips were dissolved in 6 M hydrochloric acid in order to get a 1 M final solution. Concentrated thorium chloride solutions (1.8 M) were issued from Rhodia (France) then diluted to 0.7–1.0 M.

Electron probe microanalyses (EPMA) were performed on a Cameca SX50 apparatus as described in the first part of this paper [19]. The observations of leached samples were carried out with a Hitachi S2500 scanning electron microscope.

Grazing X-ray powder diffraction diagrams were recorded with a Bruker AXS-D8 Advance diffractometer using the monochromatic CuK_α radiation ($\lambda = 1.5418$ Å) in the detector scan mode: the source position was fixed to $2\theta = 4°$ while the detector was scanning from 5° to 60°. The precise peaks positions were finally determined using the fitting program EVA, available in the software package DIFFRAC^{plus} release 2002 (Bruker AXS/SOCABIM) [22].

μ-Raman spectra were collected by the means of a Dilor–Jobin Yvon apparatus using argon laser working at 514.5 nm. The power varied from 50 to 100 mW and the laser beam was focused on the sample with an Olympus microscope.

Time resolved laser induced fluorescence spectroscopy (TRLIFS) experiments were undertaken at room temperature, using a tunable OPO panther continuum Nd:YAG (355 nm) laser as excitation source at 430 nm (with pulse of 7 ns) in order to minimize the fluorescence background coming from the solid. The detection was made by a Spectra-Pro-300 monochromator (Acton Research Corporation) coupled with a CCD camera (Princeton Instruments). As the uranyl ion fluorescence is observed in the 480–600 nm range (strong green fluorescence), the emission spectra were recorded between 450 and 600 nm using the Winspec software (Princeton Instruments). About 1000 measures were averaged to obtain these decay profiles then the time-dependence obtained was fitted using a multiexponential law.

A Philips CM30 microscope was used for TEM observations. LaB_6 filament was set at emission 2 (from a selection of 1–6) with an accelerating voltage of 300 keV in order to minimize the amorphization of the sample under the electron beam. The aperture of the condenser 2 (C2) was a 50 μm theoretical (generating an aperture angle of 1.734 mrad) and the spot size of the electron beam was 1 μm nominative. Several tests were conducted for 10 s, 1 min and 10 min of observation to estimate the best exposition time without artefacts (amorphization, bubbles, holes, ...). On this basis, sequences shorter

than 2–3 min were performed. For all the samples, the characterization was undertaken by the means of high resolution (HR) mode which allows atomic planes resolution [23,24]. All the micrographies were recorded using a Gatan slow scan camera and the Digital Micrograph software from Gatan has been used for the analysis of images. The Fourier transform was systematically done for HR micrographies to get the exact inter reticular distance of the atomic planes observed. Previously, all the micrographies were scaled from a calibration procedure at the beginning of the experiment.

2.2. Samples preparation

β-TUPD sintered pellets were prepared through the initial precipitation of TUPHPH [16] in order to improve the homogeneity of the final ceramics. These compounds were obtained by mixing concentrated thorium and uranium chloride solutions with phosphoric acid in PTFE closed containers considering the mole ratio $(U + Th)/P = 2/3$. Crystallized precursors were obtained after a heat treatment ($T = 423$–433 K) either on sand bath or in Parr Instrument Company autoclaves ($T = 433$ K, $t = 1$ month) in order to reach hydrothermal conditions. After separation of the solid from the supernatant by centrifugation at 3000 rpm, washing, drying, then using an uniaxial pressing at room temperature between 100 and 800 MPa, the pellets were fired at 1250 °C for 5–10 h in Pyrox MDB 15 or HM 40 furnaces under argon atmosphere (in order to prevent the oxidation of tetravalent uranium) [18].

2.3. Leaching tests

High density polyethylene (HDPE) containers (with low adsorption onto their surface) were considered to perform the leaching experiments from 298 to 343 K while PTFE vessels were preferred for higher temperatures. After a washing step of the samples (10^{-1} M HNO_3 or HCl, 1–7 days) to avoid the presence of crystal defects, minor phases or small particles as already described in the first part of the paper [19], the leaching tests were achieved from 298 to 393 K by mixing 100–200 mg of sintered sample with 5–25 mL of acidic solution using two kinds of experiments (called 'static' or 'dynamic' conditions). In all cases, after centrifugation of the sample at 13 000 rpm, the concentrations of thorium and uranium in the leachate were determined by Inductively Coupled Plasma Mass Spectrometry using a Fisons Plasma Quad apparatus or by PERALS alpha liquid scintillation [25] then the normalized leaching N_L (expressed in $g\,m^{-2}$) and the associated normalized dissolution rate R_L (in $g\,m^{-2}\,day^{-1}$) were determined as reported in the first part of the paper [19].

3. Results and discussion

3.1. Behavior of the actinides during the dissolution

Several leaching tests of β-TUPD sintered samples were performed in acidic media (mainly in HCl, HNO_3 and H_2SO_4) for temperatures ranging from 298 to 393 K [19]. They led to results in good agreement with that previously reported for powdered samples [15] which shows that the normalized dissolution rate determined from the uranium amount in the leachate was not significantly modified by the sintering process [19]. For all the experiments considered, both actinides exhibited different behaviors: uranium (IV) is released in the solution (due to its oxidation into uranyl) while thorium is precipitated in a phosphate-based neoformed phase (Fig. 1(a)). This precipitation occurs very quickly and is quantitative for $pH > 1$, leading to an incongruent dissolution (i.e. $r = R_L(U)/R_L(Th) > 5$) [19]. For $pH = 1$, thorium is first released in the leachate with the same normalized dissolution rate value than uranium (congruent dissolution: $r = 1$) then precipitates for leaching times ranging from 50 to 200 days, depending on the initial conditions considered. Finally, uranium(VI) is expected to precipitate for longer leaching times as the uranyl phosphate pentahydrate $(UO_2)_3(PO_4)_2 \cdot 5H_2O$. Its unit cell parameters were refined by analogy of the uranyl vanadate pentahydrate described in the literature $(UO_2)_3(VO_4)_2 \cdot 5H_2O$ [26] as already reported in our published work dealing with the leaching of β-TUPD powdered solid solutions [20].

Whatever the experimental conditions (T, pH, ...), the precipitation of thorium is correlated to a plateau in the $N_L(U)$ variation, the $R_L(U)$ value being almost equal to zero for higher leaching times (see framed part of Fig. 1(b)). This observation can be correlated to the presence of an alteration layer formed onto the surface of the leached pellet thus to the diffusion of ions from the solid to the solution through such a layer. This phenomenon was already observed on glasses and on various minerals like perlite [27,28]. In these conditions, the normalized leaching rates vary linearly with the square root of

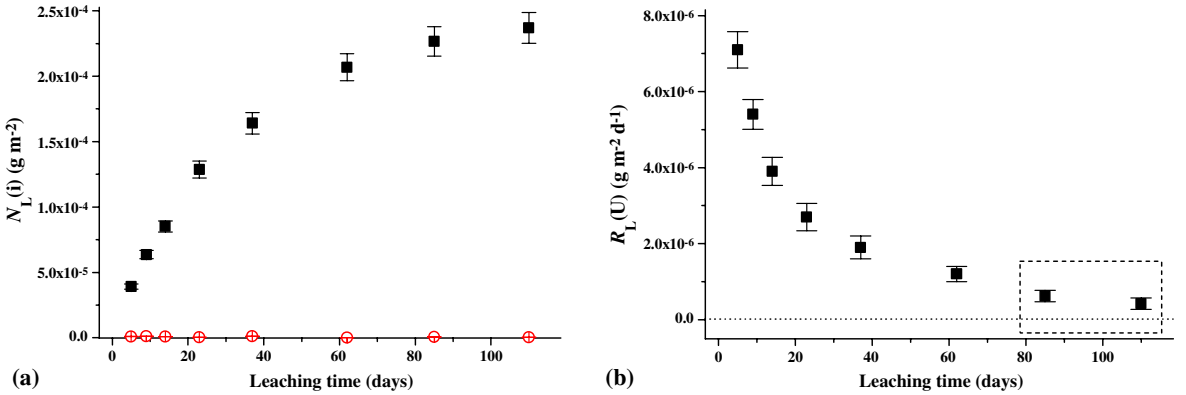

Fig. 1. Evolution of N_L(Th) (○) and N_L(U) (■) (a) and R_L(U) (b) during the leaching of β-TUPD ($x = 1.6$) in 10^{-3} M H_2SO_4 at room temperature.

time as already described in the first part of this work [19]. Besides, the formation of a neoformed phase is observed either under 'static' or 'dynamic' conditions which indicates that the precipitation probably occurs at the surface of the solid instead of from the ions present in the leachate.

3.2. Observations by SEM

In order to evidence then characterize the phases formed at the saturation of the leachate, some SEM observations were performed on leached pellets of β-TUPD ($x = 1.6$, 10^{-1} M HNO_3, $T = 363$ K, $t = 2$ months). They revealed some important modifications of the surface of the material in comparison with the raw sample [18]. The micrographies reported in Fig. 2 present four zones in the same sample, illustrating the successive steps of the dissolution process. The associated EPMA experiments are gathered in Table 1.

The inside of the sample (①) does not appear significantly modified by the aqueous alteration which confirms the good chemical durability of the β-TUPD pellets. Indeed, this zone appears very dense with no additional porosity. Moreover, its chemical composition remains almost unchanged. As it was reported previously [16], the initial slight difference observed in the uranium wt% compared to that expected comes from the synthesis process and is mainly due to the presence of small amounts of uranyl in the initial solution used for the synthesis.

The effects of dissolution are clearly observed onto the surface of the pellet. The alteration occurs preferentially inside the grain boundaries (②) and leads to the break away of the grains on 10–15 μm in depth. Simultaneously, no significant increase of the specific surface area which could accelerate the release of radionuclides from the solid to the solution, is observed from the BET-surface experiments performed on leached pellets. Moreover, EPMA results do not reveal any modification of the chemical composition which confirms that the dissolution is stoichiometric and appears in good agreement with the concentrations determined in the leachate [19].

The micrographies collected onto the surface of the leached pellet also revealed the presence of two additional phases. The first one, probably amorphous, consists of a thin layer of about 100 nm in width and appears as 'spiderwebs' (③). This morphology could result from the drying of a gelatinous phase under vacuum during the SEM experiments. More generally, this phase always appears unstable under vacuum or under electronic beam which complicates its characterization by SEM, TEM or EPMA. On the contrary, the second phase is well crystallized (④). The crystals appear as circular plates of 2–8 μm in diameter. Bigger aggregates of 10–15 μm are also observed. This morphology is similar to that of the thorium phosphate–hydrogen phosphate hydrate (TPHPH) prepared in hydrothermal conditions [29]. Thus, from all these observations, it is suggested that the solid neoformed onto the surface of the pellet is TPHPH.

Additional micrographies collected for several leaching times are presented in Fig. 3. From these observations, it appears that the amorphous phase initially formed is progressively turned into the crystallized TPHPH. For short leaching times, the precipitation of TPHPH stands in the amorphous

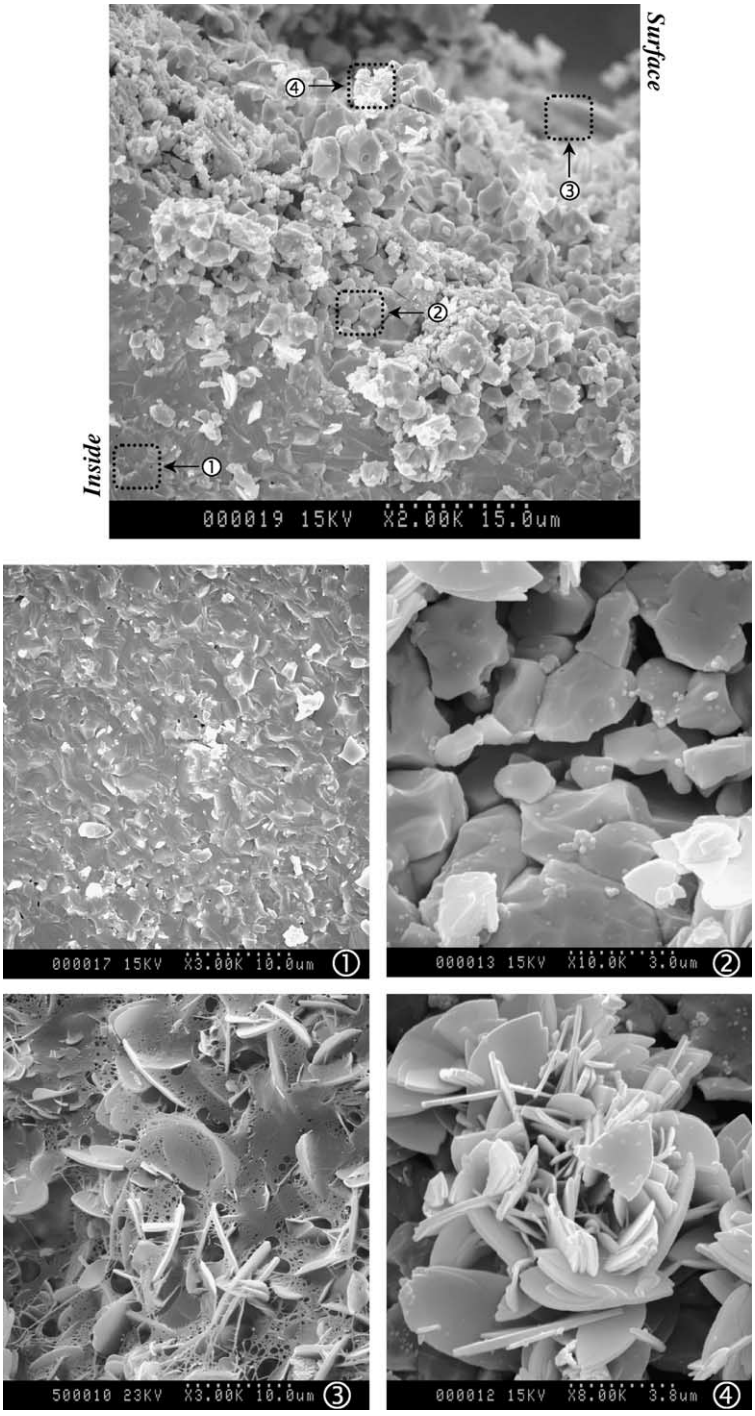

Fig. 2. SEM observations of leached β-TUPD samples ($x = 1.6$, 10^{-1} M HNO_3, $T = 363$ K, $t = 2$ months) corresponding to the successive steps of the dissolution process.

layer formed onto the surface and initially appears to be scattered. When increasing the leaching time, TPHPH crystals become more and more numerous and finally recover the entire surface of the pellet after about one year. Moreover, the precipitation of the neoformed phases also occurs in cracks and in large open pores (backscattering electron, Fig. 3(d)) where the gelatinous phase and the

Table 1
EPMA results of leached pellet of β-TUPD ($x = 1.6$, 10^{-1} M HNO_3, $T = 363$ K, $t = 2$ months)

	Th (wt%)	U (wt%)	P (wt%)	(U + Th)/PO_4	U/(U + Th)
β-$Th_{2.4}U_{1.6}P_6O_{23}$ (calc.)	37.3	25.5	12.5	0.67	0.40
Unleached sample	39.1 ± 0.8	22.8 ± 0.8	12.9 ± 0.2	0.65 ± 0.01	0.36 ± 0.01
Inside (①)	39.6 ± 0.2	22.6 ± 0.1	12.8 ± 0.1	0.65 ± 0.01	0.36 ± 0.01
Surface (②)	40.6 ± 0.7	21.8 ± 0.6	12.6 ± 0.1	0.66 ± 0.01	0.35 ± 0.01
TPHPH (calc.)	60.4	0	12.1	0.67	0
Precipitate (④)	62.2 ± 0.6	0.9 ± 0.7	12.3 ± 0.2	0.69 ± 0.01	0.02 ± 0.01

The different zones correspond to that indicated in Fig. 2.

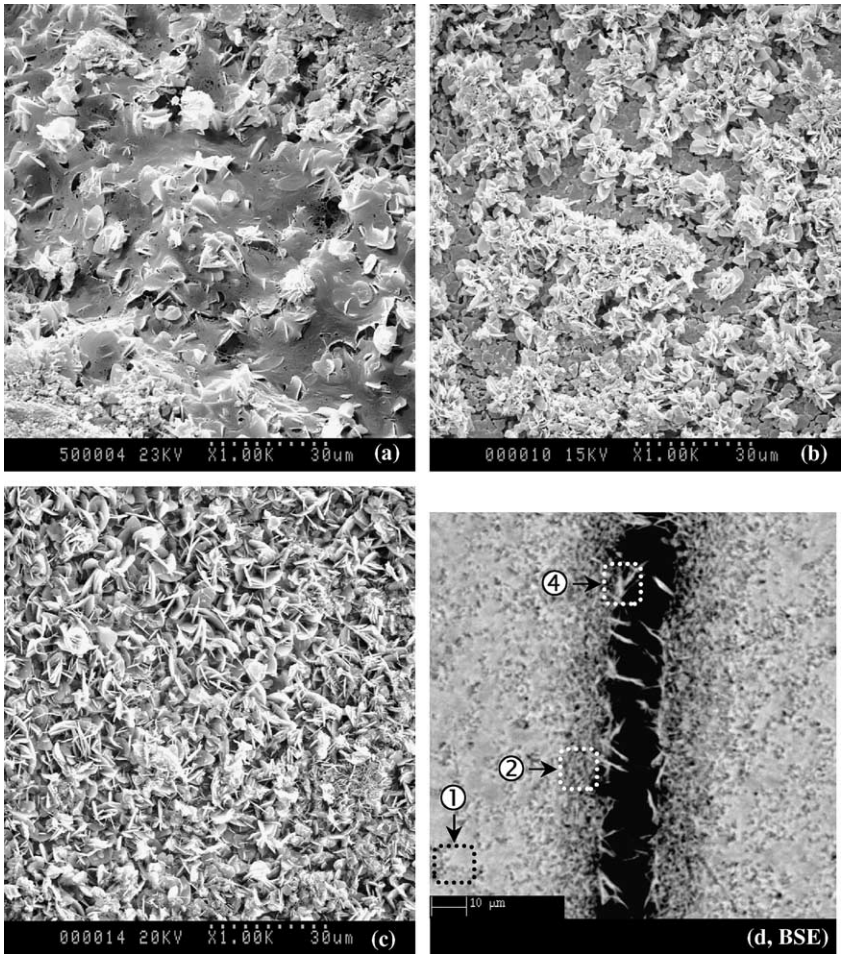

Fig. 3. SEM observations of the surface of leached β-TUPD ($x = 1.6$, 10^{-1} M HNO_3, $T = 363$ K) for increasing alteration times ((a): 1 month; (b) 3 months; (c) 1 year) and backscattering electron micrograph of a crack (d). The zones indicated on (d) correspond to that defined in Fig. 2.

TPHPH also act as protective layers. More generally, the presence of neoformed phases (amorphous and/or crystallized) will delay significantly the release of actinides in the leachate.

The EPMA results from the neoformed phases (Table 1) confirm the formation of TPHPH since the solid appears strongly uranium-depleted (mole ratio U/(U + Th) of 0.02 instead of 0.36 in the

raw material). This is consistent with the actinide concentration determined in the leachate and confirms that tetravalent uranium is preferentially released in solution consequently to its oxidation into uranyl.

3.3. μ-Raman spectroscopy

All the conclusions obtained from SEM observations and EPMA experiments were confirmed through a complete μ-Raman study. The different zones defined in the previous sections were particularly studied as shown in Fig. 4. However, since the volume analyzed was about 1 μm^3, it was not possible to collect the spectrum for each phase individually. The Raman spectrum obtained from the area covered by amorphous and crystallized neoformed phases (Fig. 4(a)) exhibits all the vibration bands characteristic of TPHPH (Table 2). That belonging to the P–O bond of the PO_4 groups can be assigned considering the data reported in the literature [29–32]: δ_s (372–428 cm^{-1}), δ_{as} (574–619 cm^{-1}), ν_s (990 cm^{-1}) and ν_{as} (1023–1150 cm^{-1}). Moreover, the presence of the vibrations of deformation of the P–O–(H) bond located at 1250 cm^{-1} in the plane and 912 cm^{-1} out of plane, confirms the existence of HPO_4 entities in the neoformed phase [33,34]. Besides, the spectrum collected from the leached sample exhibits a continuous background in the 800–1400 cm^{-1} range compared to that of well-crystallized TPHPH which also indicates the presence of the amorphous phase at the surface of the sample.

The spectrum collected on a zone of the surface free of any precipitation appears to be similar to that of unleached β-TUPD solid solution (Fig. 4(b)). All the deformation and elongation modes of the P–O bond can be observed while the bands located at 703 and 739 cm^{-1}, on the one

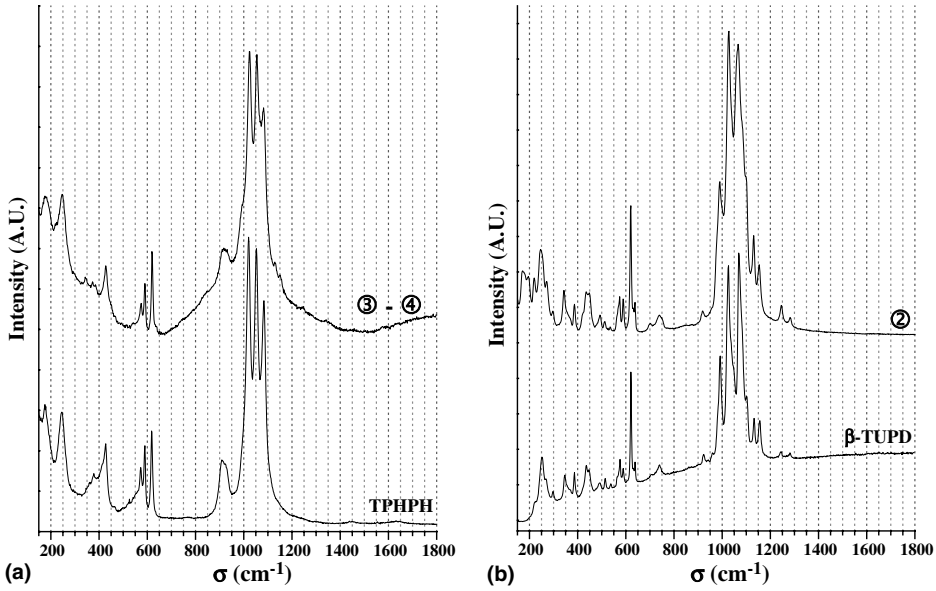

Fig. 4. μ-Raman spectra collected from the surface of leached β-TUPD ($x = 1.6$, 10^{-1} M HNO_3, $T = 363$ K, $t = 2$ months) and comparison to TPHPH (a) and to the raw β-TUPD (b). The zones indicated correspond to that already defined in Fig. 2.

Table 2
Assignment of the bands observed on the μ-Raman spectra of leached β-TUPD ($x = 1.6$, 10^{-1} M HNO_3, $T = 363$ K, $t = 2$ months) and comparison to TPHPH and to the raw β-TUPD

	δ_s (P–O)	δ_{as} (P–O)	ν_s (P–O–P)	ν_{as} (P–O–P)	ν_s (P–O)	δ_{op} (P–O–(H))	ν_{as} (P–O)	δ_{ip} (P–O–(H))
β-TUPD	346–448	490–638	706, 737	924, 942	960	–	992–1156	–
②	344–449	492–638	703, 739	919	NO	–	990–1154	–
TPHPH	362–427	572–618	–	–	957, 1000	910, 935	1025–1140	1251
③–④	372–428	574–619	–	–	990	912	1023–1150	1250

NO: Not Observed.

hand, and at 919 cm^{-1}, on the other hand, are assigned respectively to the symmetric and antisymmetric elongations of the P–O–P bridge, characteristic of P_2O_7 entities. Moreover, no additional band is detected around 850–870 cm^{-1} [35] indicating that uranium mainly remains in the tetrapositive state at the surface of the material during the dissolution. In these conditions, the oxidation of tetravalent uranium into UO_2^{2+} probably takes place in the amorphous layer.

3.4. Grazing XRD

The formation of uranium-depleted TPHPH at the surface of the β-TUPD pellets was confirmed through the characterization of several leached samples by the means of grazing XRD experiments. The XRD pattern recorded at the surface of a sample leached in 10^{-1} M HNO_3 at 363 K for 2 months is presented, as an example, in Fig. 5. It confirms the coexistence of T(U)PHPH solid solution and of residual β-TUPD. Moreover, the unit cell parameters of both structures, refined using the U-Fit software [36] correspond to $a = 21.355(7)$ Å, $b = 6.681(4)$ Å, $c = 7.025(2)$ Å and $V = 1002.3(12)$ Å^3 for T(U)PHPH and to $a = 12.783(6)$ Å, $b = 10.361(3)$ Å, $c = 7.026(2)$ and $V = 930.5(9)$ Å^3 for β-TUPD. The U/(U + Th) mole ratios, deduced from the variation of the unit cell parameters of β-TUPD and TUPHPH solid solutions versus the substitution of thorium by uranium, x_U [13,37] are found to 1.72 ± 0.09 for β-TUPD (expected value of 1.6) and 0.09 ± 0.06 for TUPHPH (expected value of 1.6). This last value slightly differs from EPMA result due to the important uncertainty generated by the weak thickness of sample analyzed in grazing XRD. Nevertheless, both techniques confirm that the chemical composition of the initial solid is not significantly modified during the dissolution process while the neoformed phase appears strongly uranium-depleted consequently to the different behaviors of thorium and uranium in the leachate.

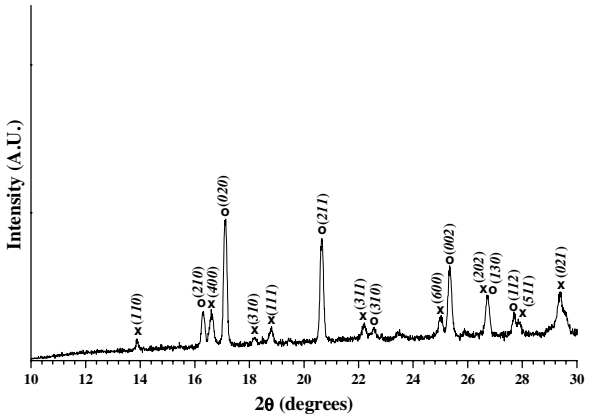

Fig. 5. Grazing XRD diagram of the surface of leached β-TUPD ($x = 1.6$, 10^{-1} M HNO_3, $T = 363$ K, $t = 2$ months). XRD lines of β-TUPD (○) and TPHPH (×).

3.5. High resolution transmission electron microscopy (HR-TEM)

The simultaneous presence of a gelatinous phase, uranium-depleted T(U)PHPH solid solution and residual sintered β-TUPD onto the surface of the leached pellets was finally confirmed through high resolution TEM observations of altered β-TUPD

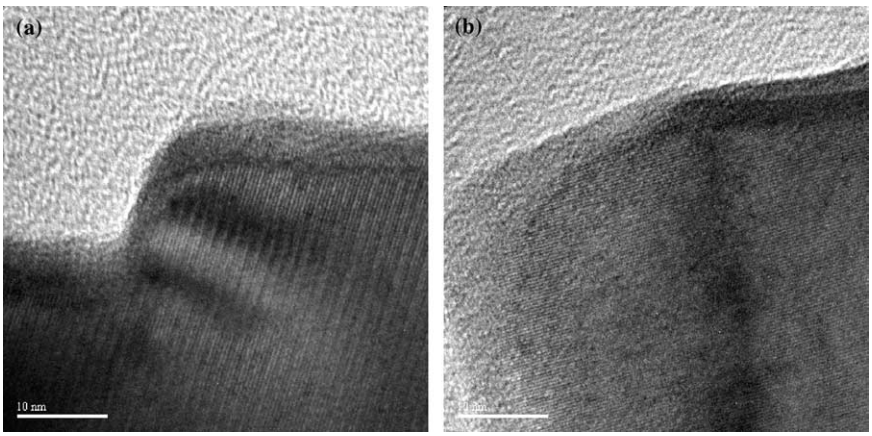

Fig. 6. High resolution TEM micrographies of β-TUPD ($x = 1.6$, 10^{-1} M HNO_3, $T = 363$ K, $t = 2$ months).

($x = 1.6$, 10^{-1} M HNO_3, $T = 363$ K, $t = 2$ months). The micrography reported in Fig. 6(a) clearly evidences the difference in crystallization state of the phases present at the surface. On the one hand, the first 10 nm do not present any lattice fringe which agrees well with an amorphous layer. On the other hand, several lattice fringes are observed in the zone corresponding to the bulk material. Moreover, since the Fourier transform of high resolution mode micrographies allows to determine the inter-reticular distances, the different fringes families observed can be assigned to the atomic planes of β-TUPD (principally 210, 211, 130, 401) or TPHPH (mainly 110, 400, 311, 600) (Table 3). Only two distances measured do not match with the theoretical values which could be due to an impurity. All other d_{hkl} values calculated appear consistent either with that of TPHPH or of β-TUPD solid solution which confirms their simultaneous presence onto the surface of the leached pellet. Moreover, both phases appear clearly segregated at the microscopic scale. In these conditions, the precipitation of uranium-depleted T(U)PHPH seems to occur mainly inside the amorphous alteration layer and probably not directly onto the surface of β-TUPD.

3.6. TRLIFS

The presence of non-constitutive uranium in the neoformed phases, as well as its oxidation state, was checked through ex situ TRLIFS experiments performed at the surface of the β-TUPD leached pellets. Even though spectrofluorimetry cannot be

Table 3
Assignment of the inter-reticular distances observed on HR-TEM micrographies of leached β-TUPD ($x = 1.6$, 10^{-1} M HNO_3, $T = 363$ K, $t = 2$ months)

HR-TEM d_{hkl} (Å)[a]	β-TUPD d_{hkl} (Å)	hkl	TPHPH d_{hkl} (Å)	hkl	Phase assignment
7.314					Not attributed
6.258	6.3975	200	6.3932	110	TPHPH or β-TUPD
5.802	5.8232	011			β-TUPD
5.503	5.4473	210			β-TUPD
5.394			5.3547	400	TPHPH
5.302	5.3001	111			β-TUPD
4.513					Not attributed
4.406	4.3064	211			β-TUPD
4.350					
4.156	4.1779	021			β-TUPD
4.112	4.0324	220			β-TUPD
4.006			4.0124	311	TPHPH
3.670			3.6089	510	TPHPH
3.637					
3.625			3.5698	600	TPHPH
3.395	3.4408	311			β-TUPD
3.382	3.3424	130			β-TUPD
3.330			3.3415	202	TPHPH
3.308	3.2961	320			β-TUPD
3.257	3.2230	112			β-TUPD
3.128			3.0815	112	TPHPH
3.116					
3.103					
3.002			3.0240	021	TPHPH
2.943			2.9397	402	TPHPH
2.922	2.9117	401			β-TUPD
2.822			2.8543	312	TPHPH
2.805	2.7945	231			β-TUPD
2.803					
2.714	2.7237	420			β-TUPD
2.687	2.6501	222	2.6773	800	β-TUPD or TPHPH
2.597	2.6501	040	2.5880	711	β-TUPD or TPHPH
2.496			2.5054	602	TPHPH
2.415			2.4254	022	TPHPH

[a] Inter-reticular distances obtained with a relative accuracy of 2%.

Table 4
Decay times of leached β-TUPD ($x = 1.6$) pellets (3–7 days) and that of some references

Sample	pH	Medium	Temperature (K)	Decay times (μs)[a]	
β-TUPD	1	HNO_3	363	84	340
β-TUPD	4	HNO_3	363	85	300
β-TUPD	Unleached samples of reference			No fluorescence	
TPHPH				No fluorescence	
TPHPH + UO_2^{2+}[b]				85	300

[a] Decay times obtained with a relative accuracy of 10%.
[b] UO_2^{2+} adsorbed onto pure TPHPH.

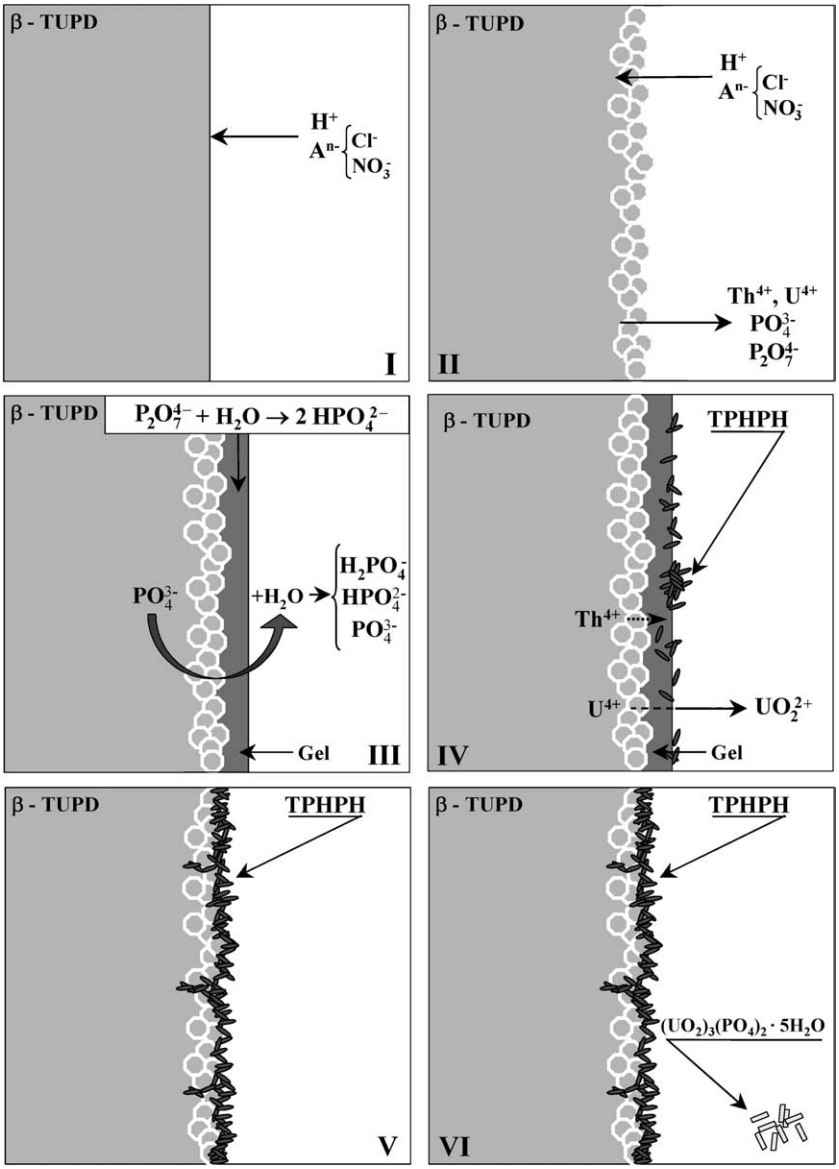

Fig. 7. Schematic representation of the dissolution of β-TUPD sintered pellets.

considered as a sensitive surface technique, the dependence of the uranium (VI) fluorescence on the chemical environment allows to use uranyl ion as a structural probe [38]. Whatever the leached

sample considered, the fluorescence spectra collected appeared consistent with those generally observed for uranyl, showing the presence of hexavalent uranium onto the surface of the solid, probably localized in the alteration layer. Moreover, since no fluorescence is observed for the unleached samples, it confirms that the oxidation of tetravalent uranium into uranyl ion only occurs during the dissolution step in the amorphous layer or in solution.

In order to confirm the nature of the neoformed phase precipitated onto the altered surface, the fluorescence decay of β-TUPD leached pellets and of uranyl adsorbed on TPHPH powdered sample were compared. In both cases, the curves are fitted with two decay times of about 80 μs and 300 μs (Table 4). In these conditions, the assumption of uranium (VI) diffusing in an alteration layer composed, among other phases, by TPHPH can be assumed. Nevertheless, these results only constitute a preliminary part of a larger work combining TRLIFS and XPS experiments. This study is actually under progress and more detailed results will be published soon.

3.7. Proposition of a mechanism scheme of the dissolution of β-TUPD sintered samples

From all the results mentioned above, the dissolution of β-TUPD sintered pellets can be schematized as reported in Fig. 7. When mixing the solid and the solution, the protons and/or the complexing ions present in the leachate start the dissolution process (**I**). This reaction occurs preferentially inside the grain boundaries, leading to the break away of grains (**II**) on 10–15 μm in depth. Nevertheless, neither the specific surface area nor the chemical composition of the sample are significantly modified. The release of the constitutive ions (i.e. U^{4+}, Th^{4+}, $P_2O_7^{4-}$ and PO_4^{3-}) in the leachate induces the formation of a gelatinous layer onto the surface of the pellet (**III**), probably due to the transformation of diphosphate entities into hydrogenphosphate groups following the reaction:

$$P_2O_7^{4-} + H_2O \Longleftrightarrow 2HPO_4^{2-} \quad (\log K\ (298\ \mathrm{K}) = 3.75\ [39]). \tag{1}$$

The release of the ions in the leachate is thus controlled by diffusion processes as shown by the straight evolution of $N_L(U)$ versus the square root of time (see the first part of this study [19]). Thus, for long leaching times, the $R_L(U)$ values become close to zero. The different behavior of actinides in the gelatinous phase depends on their redox properties: uranium (IV), oxidized in the uranyl form, is released in the leachate while thorium is quickly precipitated as TPHPH (**IV**). This precipitation leads to the destruction of the amorphous layer initially formed which progressively turns into TPHPH. These successive steps appear consistent with that observed in over-saturation conditions [40]. Beyond one year of leaching, TPHPH fully recovers the surface, the cracks and the open pores of the pellet (**V**). Moreover, as it was reported from previous work for β-TUPD powdered samples [20], uranium(VI) is finally precipitated as $(UO_2)_3(PO_4)_2 \cdot 5H_2O$ for longer leaching times (**VI**). The precipitation of such neoformed phases appears of a particular interest in the field of the immobilization of actinides for an underground repository. Indeed, by inducing the decrease of the release of actinides (normalized dissolution rates at least divided by 3), the precipitation of neoformed phases in the back-end of the initial dissolution process induces the protection of the pellet from dissolution and should delay significantly the migration of radionuclides to the solution in the context of a low leaching flow.

4. Conclusion

The characterization of β-TUPD leached pellets was undertaken in order to understand the successive steps involved in the dissolution of the material. All the experiments performed on leached pellets confirmed the good chemical durability already reported for powdered samples [15,20]. After 2 months of leaching in 10^{-1} M HNO_3, the SEM micrographies showed an alteration zone of about 10–15 μm where grains are broken away due to the relative fragility of the grain boundaries. EPMA studies did not revealed any modification of the chemical composition of the leached sample in comparison to the raw material, neither for the bulk nor for the altered zone: these results appear consistent with the stoichiometric character of the dissolution established in the first part of this paper under several operating conditions [19]. Moreover, it appears that the release of the actinides in the leachate is strongly dependent on their oxidation state: uranium is oxidized into the uranyl ion and released in the leachate while thorium remains in the tetrapositive state and quickly precipitates as neoformed phosphate-based phases. Two phases were identified at the surface of the pellets through SEM observations. First, a gelatinous phase is formed consequently

to the transformation of diphosphate entities into hydrogen phosphate groups at the surface of the pellet. In these conditions, the release of the ions in solution is driven by diffusion processes. This behavior is clearly evidenced by the straight evolution of $N_L(U)$ with the square root of time in the presence of Th-precipitation. Consequently, the amorphous layer formed onto the surface appears to be uranium-depleted and progressively turns into a crystallized compound. μ-Raman spectra collected onto the surface, as well as EPMA experiments, allow to identify this phase to the thorium phosphate–hydrogenphosphate hydrate (TPHPH). The formation of such a phase in the back-end of the initial dissolution process is expected from the incongruent behavior of the actinides studied. Nevertheless, uranium is also finally precipitated as the uranyl phosphate pentahydrate for long leaching times (over than one year). As previously presented, the precipitation of neoformed phases at saturation of the leachate induces a strong decrease of the normalized dissolution rates. Thus, the TPHPH layer formed onto the surface of the leached pellet after about one year could avoid the migration of radionuclides to the biosphere. A complementary study concerning the solubility of TPHPH and its dependence on the temperature and pH is actually under progress in order to forecast precisely its conditions of formation. Finally, since the precipitation of thorium–neptunium (IV) phosphate-hydrogenphosphate hydrate (TNpPHPH) and thorium–plutonium (IV) phosphate–hydrogenphosphate hydrate (TPuPHPH) was also observed in over-saturation conditions [41], both neptunium and plutonium could behave like thorium if their tetrapositive state is stabilized. In these conditions, the final immobilization of these tetravalent actinides in β-TPD derivative ceramics is expected to be very efficient in terms of chemical durability.

Acknowledgments

The authors would like to thank Renaud Podor and Alain Kolher from the LCSM and Thérèse Lhomme from the CREGU of the University Henri Poincaré – Nancy I (France) for performing EPMA, SEM and μ-Raman experiments. They are also grateful to J. Ritt from IRSN (France) for the ICP-MS measurements. This work was supported by the French Research Group NOMADE (GdR 2023).

References

[1] J. Carpena, F. Audubert, D. Bernache, L. Boyer, B. Donazzon, J.L. Lacout, N. Senamaud, in: I.G. McKinley, C. McCombie (Eds.), Scientific Basis for Nuclear Waste Management XXI, vol. 506, 1998, p. 543.
[2] R. Bros, J. Carpena, V. Sere, A. Beltritti, Radiochim. Acta 74 (1996) 277.
[3] L.A. Boatner, B.C. Sales, in: W. Lutze, R.C. Ewing (Eds.), Radioactive Waste Forms for the Future, North-Holland Physics Publishing, Amsterdam, 1998, p. 495.
[4] J.M. Montel, J.L. Devidal, D. Avignant, Chem. Geol. 89 (2002) 191.
[5] R. Podor, M. Cuney, Am. Miner. 765 (1997) 82.
[6] R. Podor, M. Cuney, C. Nguyen Trung, Am. Miner. 80 (1995) 1261.
[7] A. Meldrum, L.A. Boatner, W.J. Weber, R.C. Ewing, Geochim. Cosmochim. Acta 62 (1998) 2509.
[8] M.M. Abraham, L.A. Boatner, T.C. Quinby, D.K. Thomas, M. Rappaz, in: Radioactive Waste Management, vol. 1, 1980, p. 181.
[9] O. Terra, N. Clavier, N. Dacheux, R. Podor, New J. Chem. 27 (2003) 957.
[10] P. Benard, V. Brandel, N. Dacheux, S. Jaulmes, S. Launay, C. Lindecker, M. Genet, D. Louër, M. Quarton, Chem. Mater. 8 (1996) 181.
[11] V. Brandel, N. Dacheux, M. Genet, Radiokhimiya 43 (2001) 16.
[12] N. Dacheux, R. Podor, B. Chassigneux, V. Brandel, M. Genet, J. Alloys Compds. 271 (1998) 236.
[13] N. Dacheux, R. Podor, V. Brandel, M. Genet, J. Nucl. Mater. 252 (1998) 179.
[14] N. Dacheux, A.C. Thomas, V. Brandel, M. Genet, J. Nucl. Mater. 257 (1998) 108.
[15] A.C. Robisson, N. Dacheux, J. Aupiais, J. Nucl. Mater. 306 (2002) 134.
[16] N. Clavier, N. Dacheux, P. Martinez, V. Brandel, R. Podor, P. Le Coustumer, J. Nucl. Mater. 335 (2004) 397.
[17] N. Dacheux, B. Chassigneux, V. Brandel, P. Le Coustumer, M. Genet, G. Cizeron, Chem. Mater. 14 (2002) 2953.
[18] N. Clavier, N. Dacheux, P. Martinez, E. du Fou de Kerdaniel, R. Podor, L. Aranda, Chem. Mater. 16 (2004) 3357.
[19] N. Dacheux, N. Clavier, J. Ritt, J. Nucl. Mater., in press, doi:10.1016/j.jnucmat.2005.11.009.
[20] A.C. Thomas, N. Dacheux, P. Le Coustumer, V. Brandel, M. Genet, J. Nucl. Mater. 295 (2001) 249.
[21] E.H. Oelkers, F. Poitrasson, Chem. Geol. 191 (2002) 249.
[22] EVA Application 8,0,0,2, Socabim, 1996–2001.
[23] J.N. Rouzaud, A. Oberlin, M. Vandenbroucke, C.R. Somm. Soc. Geol. Fr. 5 (1978) 238.
[24] D.B. Williams, C.B. CarterTransmission Electron Microscopy, vols. I and II, Plenum, New York, London, 1996.
[25] N. Dacheux, J. Aupiais, Anal. Chem. 69 (1997) 2275.
[26] M. Saadi, C. Dion, F. Abraham, J. Solid State Chem. 150 (2000) 72.
[27] A.C. Lasaga, in: Kinetic Theory in the Earth Science, Princeton University, 1998.
[28] G. Heisbourg, PhD thesis, Université Paris-Sud-11, IPNO-T-03-09, 2003.
[29] N. Dacheux, N. Clavier, G. Wallez, V. Brandel, J. Emery, M. Quarton, M. Genet, Mater. Res. Bull. 40 (2005) 2225.

[30] A. Hezel, S.D. Ross, Spectrochim. Acta 22 (1966) 1949.
[31] P. Tarte, A. Rulmont, C. Merckaert-Ansay, Spectrochim. Acta 42A (1986) 1009.
[32] A. Rulmont, R. Cahay, M. Liégeois-Duyckaerts, P. Tarte, Eur. J. Solid State Inorg. Chem. 28 (1991) 207.
[33] A.B. Yaroslavtsev, Z.N. Prozorovskaya, V.F. Chuvaev, B.F. Parshutkin, G.G. Shifanova, Russ. J. Inorg. Chem. 34 (1989) 1188.
[34] M. Trchova, P. Capkova, P. Matejka, K. Melanova, L. Benes, J. Solid State Chem. 145 (1999) 1.
[35] J.R. Bartlett, R.P. Cooney, J. Mol. Struct. 193 (1989) 295.
[36] M. Evain, U-Fit Program, Institut des Matériaux de Nantes, France, 1992.
[37] N. Clavier, N. Dacheux, G. Wallez, M. Quarton, J. Nucl. Mater., in press.
[38] A. Kowal-Fouchard, R. Drot, E. Simoni, J.J. Ehrhardt, Environ. Sci. Technol. 38 (2004) 1399.
[39] A.C. Thomas, PhD thesis, Université Paris-Sud-11, IPNO-T-00-09, 2000.
[40] V. Brandel, N. Dacheux, M. Genet, J. Solid State Chem. 159 (2001) 139.
[41] J. Rousselle, PhD thesis, Université Paris-Sud-11, IPNO-T-04-03, 2004.